Low-Temperature Activation and Recrystallization of B^+- and BF_2^+-Implanted LPCVD Amorphous-Si Films

Huang-Chung Cheng, Fang-Shing Wang, Yeong-Fang Huang, and Chun-Yao Huang

Department of Electronics Engineering and Institute of Electronics, National Chiao Tung University, Hsinchu, Taiwan

Meng-Jin Tsai

United Microelectronics Corporation, Science-Based Industrial Park, Hsinchu, Taiwan

ABSTRACT

Low-temperature (600°C) activation and recrystallization of the low-pressure chemical vapor deposition (LPCVD) amorphous-Si films B^+- and BF_2^+-implanted with different implantation dosages and projection ranges have been investigated. The boron dopant in the amorphous-Si layer can enhance the recrystallization, resulting in the shorter incubation time and smaller grain size then the undoped specimens. For the BF_2^+-implanted specimens, the existence of fluorine atoms could postpone the grain nucleation, leading to the longer incubation time and slower nucleation rate for the heavily doped specimens than the undoped ones. For the BF_2^+-implanted specimens, as the implantation peak reaches to the α-Si/SiO_2 interface, the recoiled oxygen atoms from the oxide substrate would retard the grain nucleation and exhibit a significantly large grain size after a long time annealing. However, the recoiled oxygen atoms and the microdefects in the poly-Si layers would offset the improvement in hole mobility. Higher hole mobilities and lower trap state densities were also observed for the BF_2^+-implanted specimens with respect to the B^+-implanted ones. It is attributed to the passivation effect of fluorine atoms within the poly-Si layers.

Introduction

Polycrystalline silicon (poly-Si) deposited by the low-pressure chemical vapor deposition (LPCVD) technique is a material of great importance in microelectronics technology.[1,2] The doped poly-Si film has been employed for a variety of purposes including the interconnection lines between devices, the gate electrode materials for metal oxide semiconductor field effective transistors (MOSFETs), the resistors or poly-loads for static random access memories (SRAMs), the poly-emitter for the bipolar junction transistors,[3] and the drain/source regions for poly-Si thin film transistors (TFTs), etc. The activation of the implanted poly-Si films has been performed by using the annealing techniques such as conventional furnace annealing (CFA), [4] rapid thermal annealing (RTA), [5] as well as laser annealing (LA) [6] in high temperature regimes. Recently, in the fabrication of three-dimensional (3-D) devices and large-area microelectronics, the reduction of the process temperatures for reducing the thermal budget and the dopant redistribution of the underlayer devices becomes more important. In addition, for the thin-film transistors on glass substrates, the processing temperatures must also meet the temperature tolerance of the substrates. For the above reasons, the dopant activation at low temperature thus needs understanding.

Boron doping performed by BN diffusion source has been used for the p-type dopant in silicon devices. In recent years, ion implantation technique generally replaces traditional furnace diffusion for its precise control of implantation dosage and projection range by properly adjusting the implantation current and acceleration voltage. Both the B^+ and BF_2^+ ions are used as the p-type dopant in silicon devices and generally activated by FA or RTA methods for the temperature ranging from 700 to 1100°C. [7-9] However, the influences of the implantation dosage and projection range on the activation and grain recrystallization of B^+ and BF_2^+-implanted LPCVD amorphous-Si (α-Si) films are still unknown for the lower annealing temperatures. In this paper, low temperature activation of B^+ and BF_2^+ implanted LPCVD α-Si films with different implantation dosages and projection ranges have been studied. The BF_2^+-implanted specimens exhibit the larger hole mobilities and lower activation energies than the B^+-implanted ones. Largest grain size can also be obtained for the BF_2^+-implanted specimens as the implantation peak reach to the α-Si/SiO_2 interface. The mechanisms for the dopant activation and grain recrystallization are also proposed and discussed.

Experimental Procedures

3 in. diameter, (100) oriented, 4-7 Ω-cm, phosphorus-doped n-type Si wafers were used in this study. After the initial RCA cleaning, a thermal oxide with 500 nm in thickness was grown on the silicon wafers in a steam oxygen ambient to insulate the substrates. Undoped amorphous silicon films of 100 nm thickness were then deposited on the oxidized wafers by using an LPCVD system at 550°C. The amorphous-Si layers were then implanted with B^+ and B_2^+ ions, respectively. Implantation dosages of 4E14, 2E15, and 1E16 ion/cm^2 with the implantation peak to the half thickness of the amorphous layer were chosen for the inspection of dosage effects. To investigate the projection-range effects, implantation depth down to the α-Si/SiO_2 interface was also performed with the dosage to be 2E15 ion/cm^2. For the B^+ ions, the corresponding implantation energies to the mid and bottom regions were calculated to be 15 and 22 keV from TRIM simulation. As for the BF_2^+ ions, the acceleration voltage of 67 kV was adopted for the half-depth implantation and 98 kV for the full-depth case. After the cleaning process, the implanted samples were capped with a 200 nm plasma-enhanced chemical vapor deposition (PECVD) oxide to prevent the dopants from out-diffusion in the subsequent annealing process. The specimens were annealed in diffusion furnace with N_2 ambient at 600°C for various times. The encapsulation oxide was then dipped in a diluted HF solution. The sheet resistance, effective carrier concentration, and hole mobility of the annealed poly-Si films were determined by the four point probe and the Hall measurement apparatus with van der Pauw pattern. The crystallinity transformation was also inspected by the x-ray diffraction measurement of (111) silicon peak.[10] Poly-Si resistors with these specimens were also fabricated. The dopant profiles of the boron atoms were measured by using a CAMECA IMS-4f secondary ion mass spectroscopy (SIMS) with Cs^+ as the primary ion. The microstructure of the poly-Si grains were also observed with transmission electron microscopy (TEM) observation. Extraction of the activation energies and trap state densities from the temperature-dependence *I-V* characteristics of the poly-Si resistors were also conducted.

Downloaded on 2014-04-28 to IP 140.113.38.11 address. Redistribution subject to ECS terms of use (see ecsdl.org/site/terms_use) unless CC License in place (see abstract).

Results and Discussion

Figure 1(a) and (b) exhibits the SIMS profiles of the boron, oxygen, and silicon atoms for the 15 and 22 keV B^+-implanted specimens with the dosage of 2E15 ion/cm^2, correspondingly. The higher implantation voltage results in the deeper implantation depth. The boron tails within the SiO_2 reveal that boron ions can easily penetrate into the oxide layer. On the other hand, the SIMS profiles of boron, fluorine, oxygen, and silicon atoms for the BF_2^+-implanted specimens were shown in Fig. 2(a) and (b). It is found that the fluorine atoms have the similar distribution like the implanted boron atoms. In the inspection of oxygen distribution, a slightly graded oxygen profile near the α-Si/oxide interface has been observed for the 98 keV implantation energy with respect to that for the 67 keV one. In contrast, no significant difference in the oxygen intensity were observed between the 15 and 22 keV boron-implanted ones. It is attributed to the higher collision probability of the BF_2^+ ions with SiO_2 than that of the B^+ ones.

After the recrystallization of the implanted specimens, effects of the implantation dosage and projection range on the phase transformation were investigated using the (111) x-ray diffraction intensities, as shown in Fig. 3. The diffraction intensities of the unimplanted samples were also plotted for comparison. Regardless of the implantation dosage and energy, all of the B^+-implanted specimens display a shorter incubation time to recrystallize the amorphous phase than the unimplanted ones, as shown in Fig. 3. It is reported that the boron dopant can decrease the activation energy of the epitaxial regrowth and enhance the epitaxial regrowth rate.[11] The faster nucleation rate for the B^+-implanted samples is ascribed to the added boron atoms in the α-Si layers. As for the BF_2^+-implanted specimens, the x-ray diffraction intensities for the different implantation dosages and energies exhibit various time dependence. The medium doped films (the 4E14 ion/cm^2 case) exhibit a faster grain nucleation than the unimplanted ones. However, the longer incubation times and slower transforma-

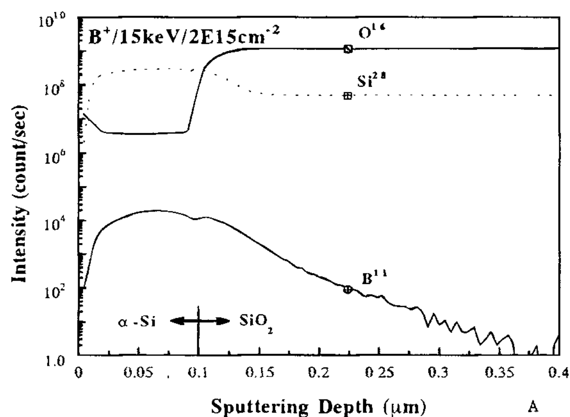

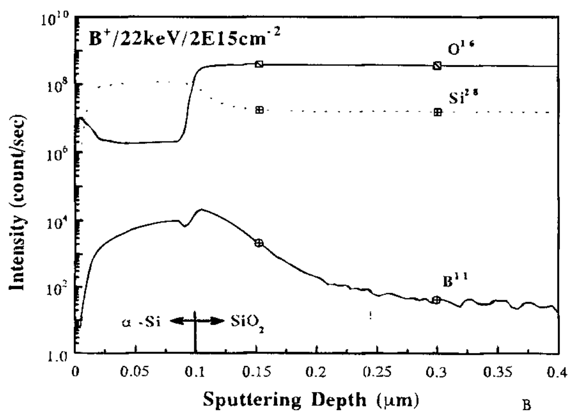

Fig. 1. The SIMS profiles of the B^+-implanted specimens with the implantation energy of (a) 15 and (b) 22 keV, respectively.

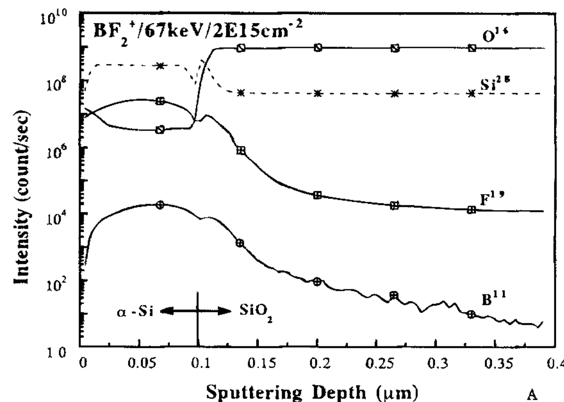

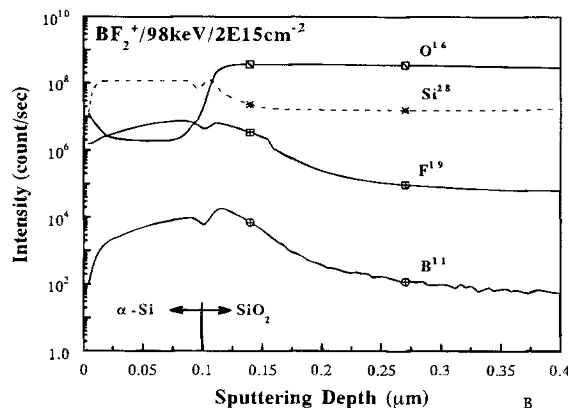

Fig. 2. The SIMS profiles of the BF_2^+-implanted specimens with the implantation energy of (a) 67 and (b) 98 keV, respectively.

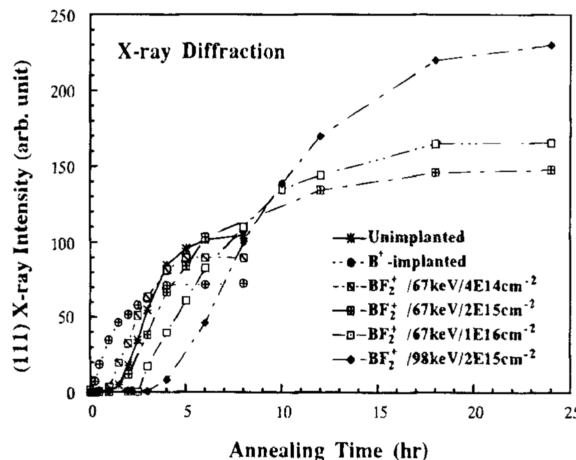

Fig. 3. The x-ray intensities of Si(111) peak for the different annealing times.

Downloaded on 2014-04-28 to IP 140.113.38.11 address. Redistribution subject to ECS terms of use (see ecsdl.org/site/terms_use) unless CC License in place (see abstract).

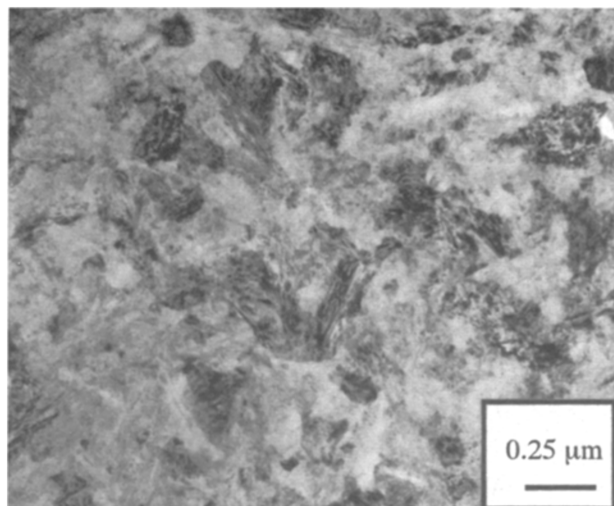

Fig. 4. Bright field (BF) micrograph of the undoped amorphous-Si for 24 h 600°C annealing.

tion rates were attained for the heavily doped specimens (the 2×10^{15} and 1×10^{16} ion/cm^2 ones). It implies that the increase of fluorine dose would postpone the grain nucleation. On the other hand, the deeply implanted case (the 98 keV one) exhibits the longest incubation time. Moreover, these specimens with slower recrystallization rates will result in higher x-ray intensities due to the larger grain size.

To understand the effects of the implantation dosage and energy on the recrystallization of the α-Si films, these specimens annealed for 24 h were also examined with TEM observation. For comparison, the microstructure of the undoped LPCVD α-Si layer was also exhibited. The dendritic grain structure with average grain size of about 0.2-0.3 μm has been observed for the undoped specimens, as shown in Fig. 4. The microstructure of the specimen B^+-implanted at 15 keV to the dosage of 2E15 ion/cm^2 was also presented in Fig. 5(a). The dendritic grains with the average grain size about 0.15-0.2 μm were observed. The grains for the 4E14 and 1E16 ion/cm^2 cases also reveal the similar structure but slightly smaller grain size for the higher dose. As can be seen, all of these B^+-implanted samples possess smaller average grain size than the undoped film. As for the 22 keV, 2E15 ion/cm^2 sample, it is found that no marked difference in the grain microstructure from the 15 keV, 2E15 ion/cm^2 one, as shown in Fig. 5(b). It means that the boron projection range does not significantly influence the grain growth of the B^+-implanted specimens. For the solid-phase recrystallization, the grain growth starts at nuclei formation and stops when the adjacent grains come into contact with each other. Hence, the lower incubation time and the faster nucleation rate for the B^+-implanted specimens would cause the smaller grain size than the undoped ones.

The grain structure of the BF_2^+-implanted specimens with the implantation dosage ranging from 4×10^{14}, 2×10^{15}, and 1×10^{16} cm^{-2} were also shown in Fig. 6(a)-(c), respectively. In contrary to the B^+-implanted cases, the grown grains reveal the larger grain size for the higher doses and ambiguous grain boundaries for the 1E16 ion/cm^2 case. As for the specimens implanted at 98 kV, the grown grains reveal the typical grain size of 0.8-1.2 μm in length, as shown in Fig. 6(d). It is significantly larger than those for all the other cases. It also agrees to the x-ray diffraction results, which show the best crystallinity for the specimens BF_2^+-implanted at 98 keV. The oxygen implanted amorphous-Si layers have been reported to possess the high activation energy and lower epitaxial growth rate.[12] Since the implantation peak will reach to the α-Si/SiO_2 interface for the 98 keV implantation, it is therefore conjectured that the recoiled oxygen atoms will incorporate with the phase transformation of the α-Si film during the recrystallization. Therefore, the lower nuclei formation for the deeply BF_2^+-implanted specimens is ascribed to the recoiled oxygen atoms from the oxide substrate. Similar results were also observed for the deeply Si^+-implanted specimens.[13]

Figure 7 shows the sheet resistances of the B^+-implanted samples with the annealing times from 12 min to 72 h. It is seen that the sheet resistance decreases dramatically within the initial 4 h. After reaching the minimum value, a slight increase for the further long annealing times was observed. The sheet resistances of the BF_2^+-implanted specimens were also shown in Fig. 8. Different from the B^+-implanted cases, the sheet resistances still stay at much higher value until the annealing times over 1 h. It implies that the fluorine atoms in the α-Si layers will postpone the boron activation in the α-Si layers. In addition, the recoiled oxygen atoms resulting from the higher implantation energy also lead to longer time delay for the dopant activation.

For a uniformly doped thin film, the sheet resistance (R_s) can be expressed as

$$R_s = 1/(N_a \times q \times \mu_{eff} \times t) \quad [1]$$

where q is the electronic charge, N_a is the average carrier concentration, μ_{eff} is the effective carrier mobility, and t is the film thickness. According to the carrier trapping model,[14] the resistivity (ρ) and the grain boundary potential barrier E_b can be expressed as

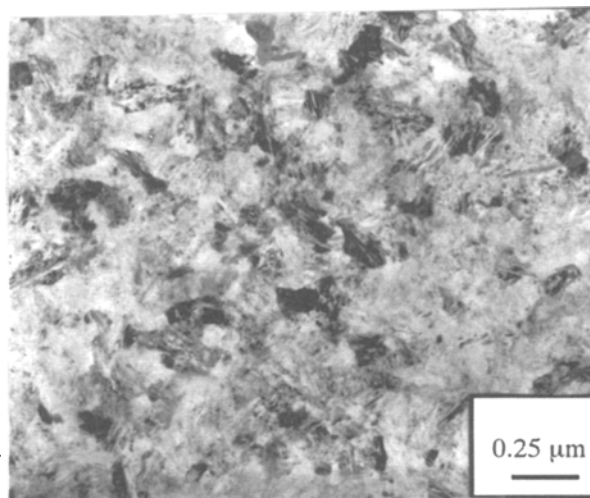

A

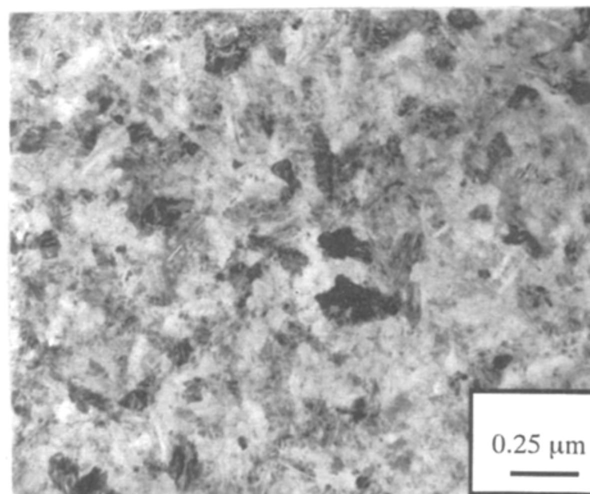

B

Fig. 5. BF micrographs of the 600°C annealed B^+-implanted specimens with dosage of (a) 2E15 ion/cm^2 at 15 keV, and (b) 2E15 ion/cm^2 at 22 keV for 24 h annealing.

Downloaded on 2014-04-28 to IP 140.113.38.11 address. Redistribution subject to ECS terms of use (see ecsdl.org/site/terms_use) unless CC License in place (see abstract).

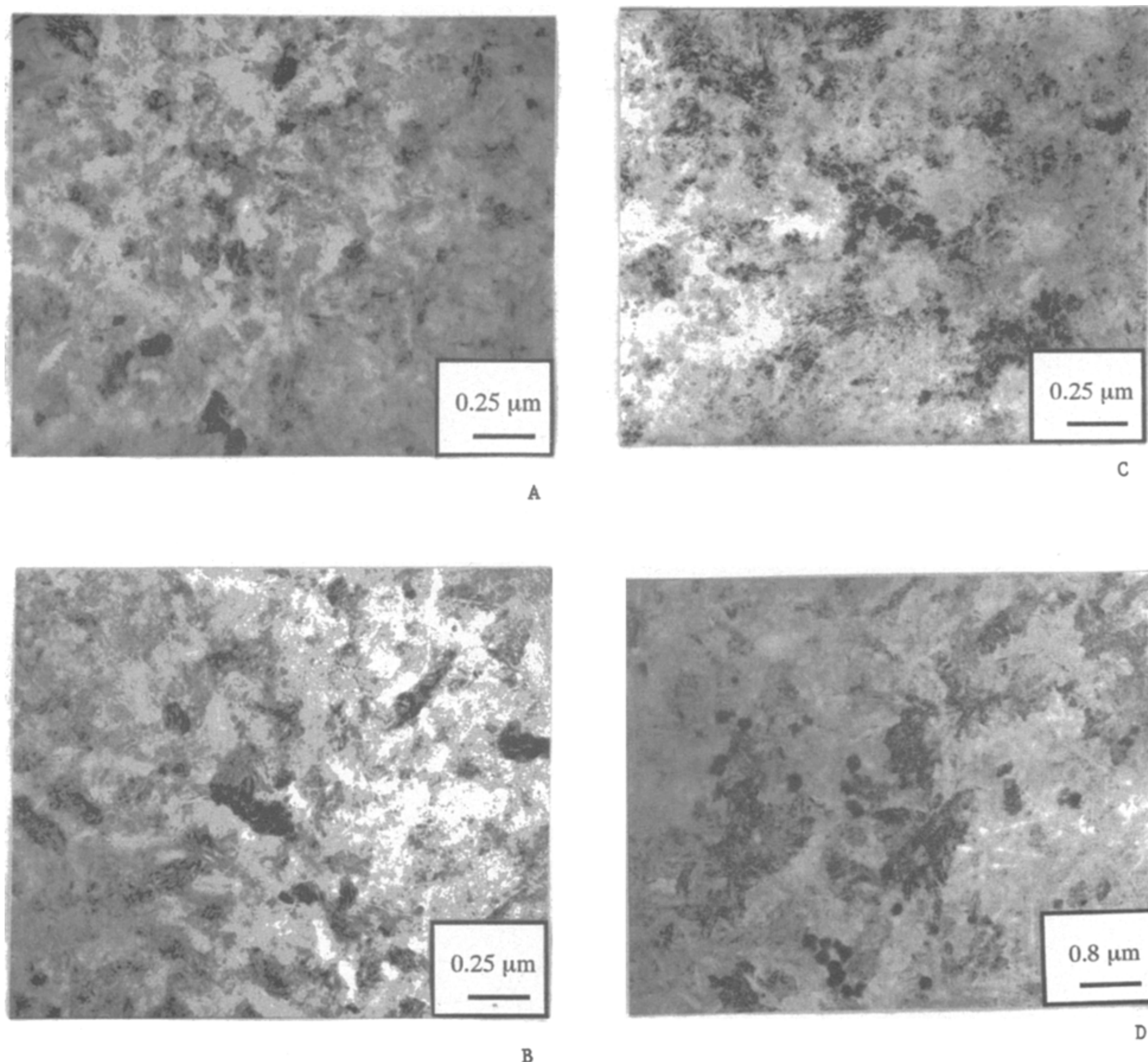

Fig. 6. BF micrographs of the 600°C annealed BF_2^+-implanted specimens with dosage of (a) 4E14 ion/cm^2, (b) 2E15 ion/cm^2, (c) 1E16 ion/cm^2 at 67 keV, and (d) 2E15 ion/cm^2 at 98 keV for 24 h annealing.

$$\rho = kT \times \exp(E_b/kT)/(q^2 \times L \times N_a \times V_c) \quad [2]$$

where k is the Boltzmann constant, T is the measuring temperature (in K), L is the grain size, and V_c is the collective velocity. As the carrier concentration N_a is higher than the trap state density N_t, the potential barrier E_b can be expressed as

$$E_b = (q^2 \times N_t^2)/(8 \times \epsilon_{Si} \times N_a) \quad [3]$$

Hence, the trap state density N_t can thus derive from the carrier concentration N_a and the grain boundary potential barrier E_b. For convenience, the temperature dependence of the poly-resistor current expressed as

$$I = I_o \times \exp(-E_b/kT) \quad [4]$$

was used for the extraction of potential barrier. Then, the trap state density is derived as the N_a value is determined by the Hall measurement.

The sheet resistance (R_s), carrier concentration (N_a), hole mobility (μ), potential barrier (E_b), trap state density (N_t), and average grain size (L) for the 24 h annealed specimens are listed in Table I. For the B^+-implanted specimens, the carrier concentration increases, but the hole mobility decreases with increasing implantation dosage. Similar dosage dependence was also observed for the BF_2^+-implanted samples. It means that the impurity scattering becomes the dominant factor to influence the carrier transport. The trap state density for the B^+-implanted samples slightly decreases with increasing doping concentration. It implied that the boron dopant could slightly passivate the trap states. As for the BF_2^+-implanted ones, a larger reduction in N_t than the B^+-implanted ones was observed. It has been reported that the existence of fluorine atoms can passivate the poly-Si trap states by forming the Si-F bonds, resulting in the better TFTs characteristics.[15] The lower trap state density for the BF_2^+-implanted specimens than the B^+-implanted ones is thus conjectured to the passivation effect of fluorine atoms. On the other hand, the carrier concentration of the BF_2^+-implanted specimens also exhibit a smaller value than the B^+-implanted ones with the same implantation dosage. The Si-F bond formation might capture some of the activation sites, leading to the lower carrier concentration and higher sheet resistance than the boron implanted ones.

As for the different projection ranges, a lower carrier concentration was observed for the deeply implanted ones. It can be realized from the larger boron tails into the oxide substrate for the higher implantation energies, as shown in Fig. 1 and 2. For the B^+-implanted specimens,

Downloaded on 2014-04-28 to IP 140.113.38.11 address. Redistribution subject to ECS terms of use (see ecsdl.org/site/terms_use) unless CC License in place (see abstract).

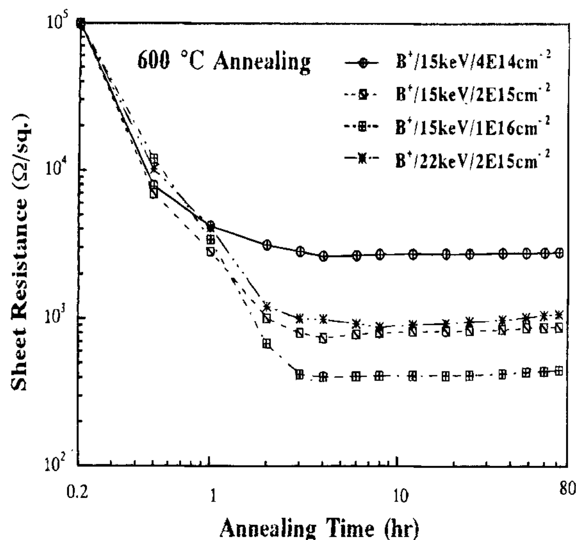

Fig. 7. The sheet resistance of the B$^+$-implanted specimens annealed at 600°C for different annealing times.

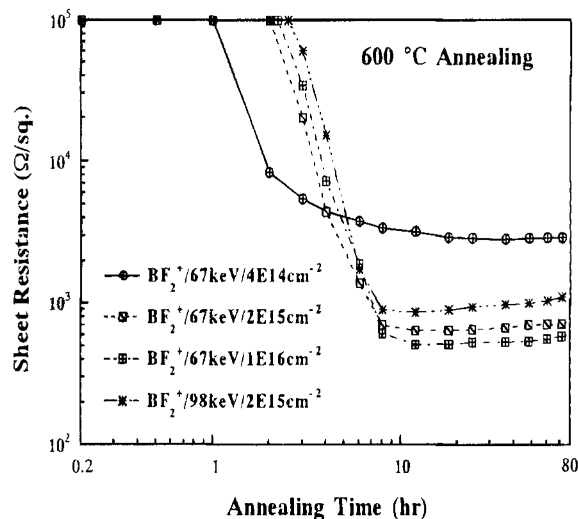

Fig. 8. The sheet resistance of the BF$_2^+$-implanted specimens annealed at 600°C for different annealing times.

the different implantation energies do not exhibit marked difference in the grain structure and electrical characteristics. As for the BF$_2^+$-implanted samples, a significantly large grain size was observed for the deeply implanted ones, as shown in Fig. 6(d). It has been explained above. However, the improvement in the hole mobility does not change correspondingly. It means that not only the grain size, but also the recoiled oxygen atoms and the grain microdefects in the poly-Si layers would influence the electrical characteristics.

Summary and Conclusions

For the B$^+$-implanted specimens, the boron dopant in the LPCVD α-Si layer can accelerate the grain nucleation, resulting in a shorter incubation time and smaller grain size than the undoped ones. As for the BF$_2^+$-implanted samples, the fluorine atoms will postpone the grain nucleation and dopant activation, resulting in the longer incubation time and slower grain growth rate for the heavily doped ones. Significantly large grain size has been observed for the deeply BF$_2^+$-implanted samples after a long time annealing. It is conjected that the oxygen atoms recoiled from the oxide substrate will cause slower nuclei formation but larger final grain size. The carrier concentration increases but the hole mobility decreases with increasing implantation dosage, reflecting that the impurity scattering is the dominant factor influencing the carrier transport. The higher hole mobility and lower trap state density for the BF$_2^+$-implanted specimens with respect to the B$^+$-implanted ones are attributed to the passivation effects of fluorine atoms in the poly-Si layers.

Acknowledgments

This research was supported in part by the Republic of China National Science Council (ROC NSC) under the Contract No. NSC-79-0404-E009-001. The technique supports from the National Nano Device Laboratory of ROC NSC and Semiconductor Research Center of National Chiao Tung University were also acknowledged.

Manuscript submitted Oct. 17, 1994; revised manuscript received July 24, 1995.

The National Chiao Tung University assisted in meeting the publication costs of this article.

REFERENCES

1. T. Kamins, *Polycrystalline Silicon for Integrated Circuit Application*, Kluwer Academic Publishers, Amsterdam (1988).
2. S. Wolf and R. N. Taauber, *Silicon Processing for the VLSI Era*, p. 161, Lattice Press, Sunset Beach, CA (1986).
3. T. H. Ning and R. D. Isaac, *IEEE Trans. Electron Devices*, **ED-32**, 242 (1980).
4. E. G. Lee and H. B. Im, *This Journal*, **138**, 3465 (1991).
5. R. A. Powell and R. Chow, *ibid.*, **132**, 194 (1985).
6. M. H. Juang and H. C. Cheng, *Appl. Phys. Lett.*, **60**, 2092 (1992).
7. A. Almaggoussi, J. Sicart, J. L. Robert, G. Chaussemy, and A. Laugier, *J. Appl. Phys.*, **66**, 4301 (1989).
8. S. R. Wilson, R. B. Gregory, W. M. Paulson, S. J. Krause, J. D. Gressett, A. H. Hamdi, F. D. Mcdaniel, and R. G. Downing, *This Journal*, **132**, 922 (1985).
9. T. Makino and H. Nakamura, *Solid-State Electron.*, **24**, 49 (1981).
10. K. T-Y. Kung and R. Reif, *J. Appl. Phys.*, **59**, 2422 (1986).
11. L. Cepregi, E. F. Kennedy, T. J. Gallagher, J. W. Mayer, and T. W. Sigmon, *ibid.*, **48**, 4234 (1977).
12. G. Foti, J. C. Bean, J. M. Poate, and C. W. Magee, *Appl. Phys. Lett.*, **36**, 840 (1980).
13. I.-W. Wu, A. Chiang, M. Fuse, L. Ovecoglu, and T. Y. Huang, *J. Appl. Phys.*, **65**, 4036 (1989).
14. G. Baccarani, B. Ricco, and G. Spadini, *ibid.*, **49**, 5565 (1978).
15. H. N. Chern, C. L. Lee, and T. F. Lei, *IEEE Trans. Electron Devices*, **ED-41**, 698 (1994).

Table I. The sheet resistance (R_s), carrier concentration (N_a), hole mobility (μ), potential barrier (E_b), trap state density (N_t), and average grain size (L) of the specimens annealed for 24 h.

Samples \ Parameters	R_s (Ω/□)	N_a (1/cm^3)	μ (cm^2/V · s)	E_b (eV)	N_t (1/cm^2)	Grain size L (μm)
B$^+$/15 keV/4E14 cm^{-2}	2783	2.9E19	7.8	0.1	1.23E13	0.15 − 0.2
B$^+$/15 keV/2E15 cm^{-2}	818	1.27E20	6.0	0.002	1.16E13	0.15 − 0.2
B$^+$/15 keV/1E16 cm^{-2}	437	3.60E20	4.1	0.006	1.07E13	0.1 − 0.15
B$^+$/22 keV/2E15 cm^{-2}	1000	1.0E20	6.3	0.026	1.17E13	0.15 − 0.2
BF$_2^+$/67 keV/4E14 cm^{-2}	2860	2.7E19	8.1	0.08	1.07E13	0.15 − 0.2
BF$_2^+$/67 keV/2E15 cm^{-2}	840	1.14E20	6.5	0.009	7.35E12	0.2 − 0.3
BF$_2^+$/67 keV/1E16 cm^{-2}	480	3.0E20	4.4	0.0026	6.41E12	0.2 − 0.3
BF$_2^+$/98 keV/2E15 cm^{-2}	1040	9.1E19	6.7	0.008	6.20E12	0.8 − 1.2

Downloaded on 2014-04-28 to IP 140.113.38.11 address. Redistribution subject to ECS terms of use (see ecsdl.org/site/terms_use) unless CC License in place (see abstract).